Calhoun: The NPS Institutional Archive

DSpace Repository

Faculty and Researchers | Faculty and Researchers' Publications

1993-10-01

An inviscid-viscous interaction approach to the calculation of dynamic stall initiation on airfoils

Cebeci, T.; Platzer, M.F.; Jang, H.M.; Chen, H.H.

Journal Name: Journal of Turbomachinery; (United States); Journal Volume: 115:4
https://hdl.handle.net/10945/61055

This publication is a work of the U.S. Government as defined in Title 17, United States Code, Section 101. Copyright protection is not available for this work in the United States.

Downloaded from NPS Archive: Calhoun

http://www.nps.edu/library

Calhoun is the Naval Postgraduate School's public access digital repository for research materials and institutional publications created by the NPS community. Calhoun is named for Professor of Mathematics Guy K. Calhoun, NPS's first appointed -- and published -- scholarly author.

Dudley Knox Library / Naval Postgraduate School
411 Dyer Road / 1 University Circle
Monterey, California USA 93943

THE AMERICAN SOCIETY OF MECHANICAL ENGINEERS
345 E. 47 St., New York, N.Y. 10017

92-GT-128

The Society shall not be responsible for statements or opinions advanced in papers or in discussion at meetings of the Society or of its Divisions or Sections, or printed in its publications. Discussion is printed only if the paper is published in an ASME Journal. Papers are available from ASME for fifteen months after the meeting.
Printed in USA.

Copyright © 1992 by ASME

An Inviscid-Viscous Interaction Approach to the Calculation of Dynamic Stall Initiation on Airfoils

T. CEBECI
Aerospace Engineering Department
California State University, Long Beach, Long Beach, CA

M. F. PLATZER
Department of Aeronautics and Astronautics
Naval Postgraduate School, Monterey, CA

H. M. JANG and H. H. CHEN
Aerospace Engineering Department
California State University, Long Beach, Long Beach, CA

ABSTRACT

An interactive boundary-layer method is described for computing unsteady incompressible flows over airfoils, including the initiation of dynamic stall. The inviscid unsteady panel method developed by Platzer and Teng is extended to include viscous effects. The solutions of the boundary-layer equations are obtained with an inverse finite-difference method employing an interaction law based on the Hilbert integral, and the algebraic eddy-viscosity formulation of Cebeci and Smith. The method is applied to airfoils subject to periodic and ramp-type motions and its abilities are examined for a range of angles of attack, reduced frequency and pitch rate.

1.0 INTRODUCTION

The effect of unsteady motion of an airfoil on its stall behavior is of considerable interest regarding propellers, helicopter rotors and compressors. Experiments with oscillating airfoils (Carr, 1988) have shown that the flow remains attached for angles of attack greater than those which cause stall on a steady airfoil. In addition, the onset of dynamic stall depends on the airfoil geometry, the flow Reynolds number and Mach number, and on the degree of flow unsteadiness (reduced frequency). Hence there is a great need to develop calculation methods which can predict this phenomenon.

In principle there are two approaches to the calculation of viscous unsteady flows, one based on the solution of the Reynolds-averaged Navier-Stokes equations or their reduced forms and the other on the solution of a combination of inviscid and boundary-layer equations, often referred to as the interactive boundary-layer approach. Both calculation approaches have merit when applied to airfoil and wing flows, though the more complete Navier-Stokes equations are likely to better represent those flows in which cross-stream convection and diffusion are important, as in fully stalled conditions, whereas the interactive approach offers the possibility of more accurate numerical solutions with considerable savings of computer time and storage. An appraisal of either calculation method must also be viewed in the context of the physical processes which they are to represent. Thus, in the case of unsteady airfoil flows, we are concerned with boundary layers which are comparatively thin at moderate angles of attack, thicker at higher angles of attack with regions of separation on the upper surface of the airfoil, formation of a vortex at much higher angles of attack followed by rather thick and separated flow. Transition, with its complicated dependence upon geometry, becomes increasingly more important with increasing angle of attack and with decreasing chord Reynolds number. All these effects occur close to a surface so that the calculation method must represent a comparatively thin layer with high accuracy.

This paper presents an efficient and accurate approach for calculating unsteady flows over airfoils. It is based on the interactive boundary-layer approach that has been explored extensively for steady airfoil flows by Cebeci, et al. (1986), (1990) and (1991). Comparisons between the predictions of this method for steady flows include experimental data and solutions of the Navier-Stokes equations by Mehta, et al. (1986) and Chang, et al. (1988). Recently Jang et al. (1990) extended the interactive approach to the calculation of blade boundary layers and compared its predictions with Navier-Stokes calculations. In the present paper, in Section 2, we provide a complete description of this method including its extension to the prediction of dynamic stall onset on airfoils subject to ramp-type or harmonic oscillation motions. Results are presented in the third section and the paper ends with a summary of the more important conclusions.

2.0 INTERACTIVE METHOD FOR UNSTEADY FLOWS

As in two-dimensional steady flows, the interactive method for unsteady flows is based on the solutions of the inviscid and boundary-layer equations so as to ensure that each influences the other. The inviscid flow equations are solved by a panel method in which the airfoil is defined by a set of points with neighboring points connected by straight-line panels which have source density q_j ($j = 1, 2, \ldots, n$) and vorticity γ. The inviscid method, developed by Platzer

Presented at the International Gas Turbine and Aeroengine Congress and Exposition
Cologne, Germany June 1-4, 1992
This paper has been accepted for publication in the Transactions of the ASME
Discussion of it will be accepted at ASME Headquarters until September 30, 1992

Downloaded From: https://proceedings.asmedigitalcollection.asme.org on 01/24/2019 Terms of Use: http://www.asme.org/about-asme/terms-of-use

and Teng (1987) is essentially an extension of the well-known Hess-Smith panel method for steady flows (Hess and Smith, 1966). The induced velocities caused by the elementary flows corresponding to source and vortex flows satisfy the irrotationality condition and the boundary conditions at infinity. In the approach adopted by Hess and Smith (1966), the source strength is assumed to be constant over each panel and is adjusted to give zero normal velocity over the airfoil and the vorticity strength is taken to be constant on all panels with its single value adjusted to satisfy the condition associated with the specification of circulation. The Kutta condition is used for this purpose, and although several properties of the flow at the trailing edge have been used in lieu of this condition, in the Hess-Smith method it is assumed that the upper and lower surface tangential velocities approach a common limit at the trailing edge.

In the extension of this method to unsteady flows, it is again necessary to determine the surface singularity distributions of source q_j and vorticity γ. We have the same number of unknowns, (n + 1), but they are time-dependent. We, therefore, introduce a subscript k as the time-step counter so that the unsteady flow problem is postulated to be solved at successive intervals of time, starting from $t_0 = 0$. At each time step, t_k (k = 1, 2, ...), the airfoil is represented by surface singularity distributions consisting of source and vorticity distributions $(q_j)_k$ (j = 1, 2, ..., n) and γ_k. Again the source strengths vary from panel to panel but the vorticity strength remains the same for all panels.

The overall circulation Γ_k at time-step t_k is γ_k multiplied by the airfoil perimeter, ℓ, and since the total circulation must be conserved according to the Helmholtz theorem of conservation of vorticity, any changes in the circulation at the airfoil surface must be balanced by an equal and opposite change in the vorticity leaving the airfoil. This vortex shedding process takes place through an element attached as an additional panel at the trailing edge with uniform vorticity distribution $(\gamma_w)_k$. This shed vorticity panel is established if its length Δ_k and inclination to the x-axis of the airfoil-fixed coordinate system θ_k are determined. These are determined with the procedure of Basu and Hancock (1987) and the shedding process from the trailing edge is represented by a series of free vortices, each of constant vorticity determined by the time history of the circulation about the airfoil.

The viscous effects are included in the inviscid method through a blowing velocity, v_n

$$v_n = \frac{d}{dx}(u_e \delta^*) \tag{1}$$

which replaces the zero normal velocity at the airfoil surface and through the application of the Kutta condition. The blowing velocity displaces the dividing streamline outward from the surface of the airfoil to the location of the displacement thickness. The blowing velocity applied on the airfoil is replaced by suction velocity placed on the wake dividing streamline, as is the case for steady flows. Experience has shown that best results are obtained when surface pressures are calculated with a Kutta condition applied on the displacement surface rather than on the surface panels.

The boundary-layer equations for two-dimensional incompressible laminar and turbulent flows are well known and, with the eddy viscosity (ϵ_m) concept, can be expressed in the following form

$$\frac{\partial u}{\partial x} + \frac{\partial v}{\partial y} = 0 \tag{2}$$

$$\frac{\partial u}{\partial t} + u\frac{\partial u}{\partial x} + v\frac{\partial u}{\partial y} = \frac{\partial u_e}{\partial t} + u\frac{\partial u_e}{\partial x} + \nu\frac{\partial}{\partial y}\left(b\frac{\partial u}{\partial y}\right) \tag{3}$$

where $b = 1 + \epsilon_m/\nu$. The usual wall boundary conditions on the airfoil are

$$y = 0, \quad u = v = 0 \tag{4a}$$

For an external velocity distribution specified by the panel method, $u_e^0(x,t)$, the edge boundary condition is

$$y = \delta, \quad u = u_e^0(x,t) \tag{4b}$$

The boundary conditions in the wake, as in steady flows, require the definition of a dividing line, $y = y_0$, which in our study is assumed to correspond to the instantaneous wake dividing streamline. This may not be a good choice for severe unsteady motions but is likely to be appropriate for mild unsteady motions. The resulting boundary conditions in the wake are

$$y = y_0, \quad v = 0 \tag{5a}$$

$$y \to \pm\infty, \quad u \to u_e^0(x,t) \tag{5b}$$

To calculate flows with separation, the external velocity must be computed as part of the solution. In the present study, as in steady flows, this is achieved with the formulation recommended by Veldman (1981), according to which the perturbation velocity due to viscous effects, namely, $\delta u_e(x,t)$ will be assumed to be given by the so-called Hilbert integral,

$$\delta u_e(x,t) = \frac{1}{\pi}\int_{x_a}^{x_b} \frac{d}{d\sigma}(u_e\delta^*)\frac{d\sigma}{x-\sigma} \tag{6}$$

in the interaction region confined to the range $x_a \le x \le x_b$ so that the edge boundary condition (5b) is written as

$$u_e(x,t) = u_e^0(x,t) + \delta u_e(x,t) \tag{7}$$

In addition to the above boundary conditions, the solution of Eqs. (2) and (3) require initial and upstream conditions. We generate the former by assuming that at t = 0 steady conditions prevail and solve the steady-flow equations. There is no problem in generating the upstream conditions for the steady-flow equations since the calculations start at the stagnation point. However, the situation is somewhat different for unsteady flows since the stagnation point is not fixed and, although u_e is zero, we cannot assume a priori that u is also zero. A convenient and accurate procedure to calculate the first velocity profile (the upstream condition) at the new time step has been developed by Cebeci and Carr (1983). This procedure involves the characteristic box scheme developed by Cebeci and Stewartson, as described in Bradshaw et al. (1981) and is used to generate the upstream conditions.

A detailed description of the solution procedure will be reported separately. Briefly, the above equations employing the algebraic eddy-viscosity formulation of Cebeci and Smith (1974) are first expressed in transformed coordinates; these provide significant advantages over the physical coordinates by allowing the calculations to be performed with larger steps in the streamwise and time directions. In addition, they remove the singularity the equations have in physical coordinates at the stagnation point of the airfoil.

Downloaded From: https://proceedings.asmedigitalcollection.asme.org on 01/24/2019 Terms of Use: http://www.asme.org/about-asme/terms-of-use

Two sets of coordinate transformations are employed, one for the direct problem when the equations are solved for the prescribed pressure distribution and the other for the inverse problem with the inviscid velocity updated during the iterations. In the direct mode we use the Falkner-Skan transformation given by

$$\eta = \sqrt{u_e/\nu x}\, y, \qquad \psi = \sqrt{u_e \nu x}\, f(x,\eta) \tag{8}$$

and write Eqs. (2) and (3) in the following form

$$(bF'')' + \frac{m+1}{2} FF'' + m[1 - (F')^2] + m_3(1 - F') - \frac{1}{2} m_3 F''$$

$$= x\left(\frac{1}{u_e}\frac{\partial F'}{\partial t} + F'\frac{\partial F'}{\partial x} - F''\frac{\partial F}{\partial x}\right) \tag{9}$$

Here a prime denotes differentiation with respect to η and m and m_3 are dimensionless pressure gradient parameters given by

$$m = \frac{x}{u_e}\frac{\partial u_e}{\partial x}, \qquad m_3 = \frac{x}{u_e^2}\frac{\partial u_e}{\partial t} \tag{10}$$

In the inverse mode, we use a modified form of the transformation given by Eq. (8),

$$Y = \sqrt{u_o/\nu x}\, y, \qquad \psi = \sqrt{u_o \nu x}\, f(x,y) \tag{11}$$

and, with a prime now denoting differentiation with respect to Y, write Eqs. (2) and (3) in the following form

$$(bf'')' + \frac{1}{2} ff'' + xu_e\frac{\partial u_e}{\partial x} + x\frac{\partial u_e}{\partial t}$$

$$= x\left(\frac{\partial f'}{\partial t} + f''\frac{\partial f'}{\partial x} - f''\frac{\partial f}{\partial x}\right) \tag{12}$$

In the direct mode, the boundary conditions for Eq. (9) are straightforward and follow from those given by Eqs. (4) and (5). For airfoil calculations, they are

$$\eta = 0, \quad F = F' = 0; \quad \eta = \eta_e, \quad F' = 1 \tag{13a}$$

and for wake calculations, they are

$$\eta = \eta_o, \; F = 0; \quad \eta \to \pm\infty, \quad F' \to 1 \tag{13b}$$

In the inverse mode, after applying a discrete approximation to the Hilbert integral, those on the airfoil are

$$Y = 0, \quad f = f' = 0 \tag{14a}$$

$$Y = Y_e, \quad u_e - \tilde{c}_{ii}(Y_e u_e - f_e) = g_i \tag{14b}$$

and in the wake

$$Y = \pm Y_e, \quad u_e - \tilde{c}_{ii}[u_e(Y_e - Y_{-e}) - (f_e - f_{-e})] = (g_w)_i \tag{15a}$$

$$Y = Y_o, \quad f = 0 \tag{15b}$$

In the above equations, the subscript e denotes quantities at the edge of the wall boundary layer and the upper edge of the wake; $_{-e}$ denotes quantities at the lower edge of the wake; $\tilde{c}_{ii}$ is defined as

$$\tilde{c}_{ii} = c_{ii}\left(\frac{\nu}{u_o}\right)^{1/2} \tag{16}$$

The parameters g_i and $(g_w)_i$ are given by

$$g_i = (u_e^o)_i^k + \sum_{j=i_a^I}^{i-1} C_{ij}[D_j^I - (D_j^I)^k]$$

$$- C_{ii}(D_i^I)^k + \sum_{j=i+1}^{i_b} C_{ij}[DB_j^I - (D_j^I)^k] \tag{17a}$$

$$(g_w)_i = (u_e^o)_i^k + \frac{1}{2}\sum_{I=u\&l}\left\{\sum_{j=i_a^I}^{i-1} C_{ij}[D_j^I - (D_j^I)^k]\right.$$

$$\left. - C_{ii}(D_i^I)^k + \sum_{j=i+1}^{i_b} C_{ij}[DB_j^I - (D_j^I)^k]\right\} \tag{17b}$$

where the superscript I=u refers to upper side quantities or l to lower side quantities, with

$$D \equiv \sqrt{\nu/u_o}\,(Y_e u_e - f_e)$$

Depending on the complexity of the flowfield, two forms of the box scheme are employed. In regions where u is positive, the regular box scheme is used. In regions of negative u velocity, the characteristic box scheme is used with the FLARE approximation, discussed in Bradshaw et al. (1981) in which the convective term in the momentum equation, $f''(\partial f'/\partial x)$ is set equal to zero in regions of negative velocity. Further details will be provided by Cebeci and Khattab (1992).

3.0 RESULTS AND DISCUSSION

For a given inviscid velocity distribution provided by the panel method, the solutions of the boundary-layer equations described in the previous section involve an iteration process in which the downstream effects are accounted for by performing a series of calculations (sweeps) on the airfoil and in the wake starting first on the stagnation point of the airfoil. After each sweep, the displacement thickness is updated so that the upstream and downstream viscous effects can be included in the next sweep. In addition to improving the boundary-layer calculations in this way, the effect of viscous effects on the pressure distribution are also accounted for via the blowing velocity in the panel method. Moreover, for the flow over a lifting body, the Kutta condition and wake-vorticity effects are related to the pressure distribution on the body surface.

The calculations start with the steady-state conditions and upon the convergence of the solutions, the same iterative procedure shifts to the next time step with the solutions at previous time as initial guesses. A typical evolution of the solutions during the inviscid-viscous iteration procedure is shown in Figs. 1 and 2. The calculations were performed for the Sikorsky SSC-A09 airfoil section at a chord Reynolds number of 2×10^6 and an angle of attack of 15°, which is beyond that of maximum lift. In order to

Downloaded From: https://proceedings.asmedigitalcollection.asme.org on 01/24/2019 Terms of Use: http://www.asme.org/about-asme/terms-of-use

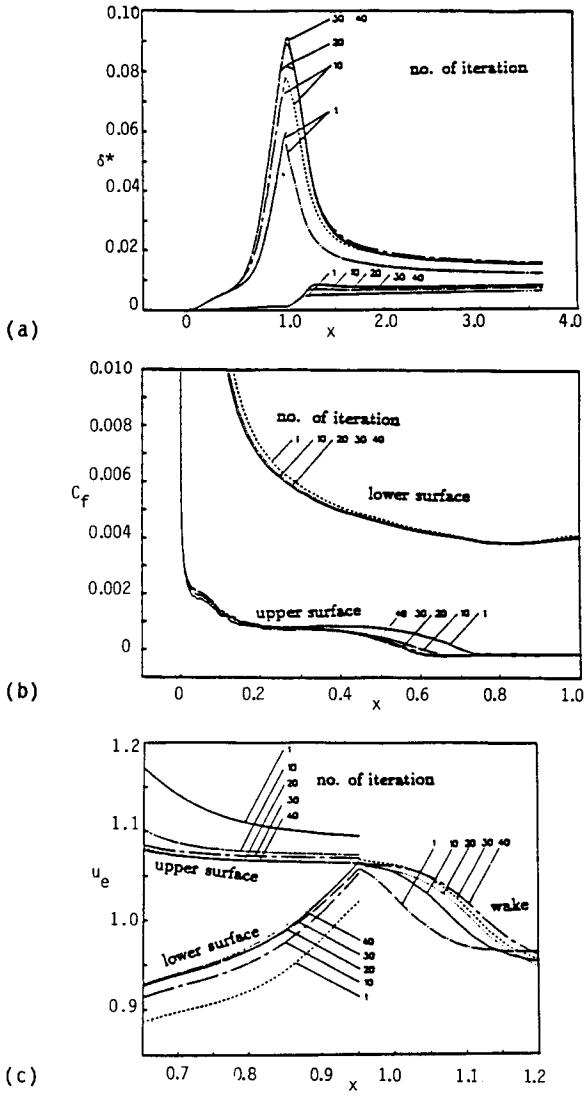

Fig. 1. The variation of the (a) displacement-thickness, (b) local skin-friction coefficient, and (c) boundary-layer edge velocity (only the trailing-edge region are shown) distributions with iteration number. - Steady, $\alpha = 15°$, $R_c = 2 \times 10^6$.

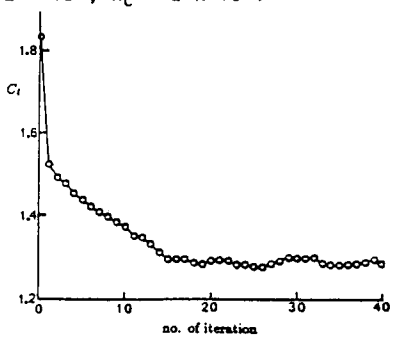

Fig. 2. The variation of lift-coefficient with iteration number. - Steady, $\alpha = 15°$, $R_c = 2 \times 10^6$.

improve the rate of convergence, the calculations began with displacement thickness and blowing-velocity distributions from a converged solution at an angle of attack of 14° so that the solutions indicated by iteration 1 in Fig. 1 include viscous effects. Figure 1(a) shows the upper surface, lower surface and wake displacement-thickness distributions. The displacement thickness on the lower surface and for the forward 0.4 of chord on the upper surface do not change with the iterations, whereas the trailing-edge displacement thickness on the upper surface increases by 50 percent during the computation. Figure 1(b) illustrates the change in local skin-friction coefficients with iteration number on the two surfaces; the only important changes are in the vicinity of separation. The variation of the velocity distribution, u_e, with iteration is shown in Fig. 1(c), and it should be noted that the discontinuities in the u_e and δ^* distributions at the trailing edge are gradually eliminated as the iteration number increases.

For the results presented in this paper, twenty inviscid-viscous iterations were assumed to be sufficient for flows involving stall, and fewer iterations were sufficient where stall did not occur. The variation of lift coefficient with iterations is shown in Fig. 2, and the large change in the first iteration is due to the initial guess.

The interactive boundary-layer calculations can be performed for an airfoil with and without consideration of its wake. Before we present results for an airfoil operating under unsteady flow conditions, we first consider the wake effect on the solutions. To this end, we examine the Sikorsky SSC-A09 airfoil undergoing a harmonic oscillation, $\alpha = 5° + 7° \sin(\omega t)$, at a very low reduced frequency, $k(\equiv \omega c/2u_\infty) = 1 \times 10^{-5}$. The lift coefficients of Fig. 3a show that for a chord Reynolds number, R_c, of 2×10^6, the roles of wall boundary layer and viscous wake are opposite so that the former reduces the lift coefficient while the latter increases it, and the magnitudes of the effects increase at high angles of attack. Figure 3b shows the displacement thicknesses on the upper and lower surfaces at the trailing edge for one cycle of motion, and Fig. 3c shows the displacement thickness distribution on the upper surface at various angles of attack. Both figures show that the viscous wake reduces the displacement thickness which is built up by the viscous effects in the wall boundary layer.

The study of the viscous wake effects in the slow motion cases, as described above, provides a quantitative standard for evaluating the viscous wake effects in more severe unsteady flows. When the airfoil performs slow movements, the vorticities shed to the wake are weak and the wake, due to the viscosity, behaves like a distribution of sinks along the dividing line. Increasing the severity of the unsteady motion increases the strength of the vorticities shed to the wake. The wake of a real flow over an airfoil can, therefore, be described as including vorticities and sinks which mix and interact with each other.

To model the unsteady wake by a viscous-inviscid interactive method, some assumptions are necessary. In the present method we have assumed that the two elements of the unsteady wake model, vorticities and sinks, are distinct and do not influence each other. This means that the vorticities shed via the potential flow go downstream according to their own local velocities without the influence of sinks, and the sinks computed from the viscous wake distribute on the instantaneous wake dividing line, the location of which is evaluated without the influence of vorticities. This model satisfies the steady-flow condition as the unsteady motion approaches zero and should capture most of the characteristics of the wake as the unsteady motion of the airfoil increases.

Downloaded From: https://proceedings.asmedigitalcollection.asme.org on 01/24/2019 Terms of Use: http://www.asme.org/about-asme/terms-of-use

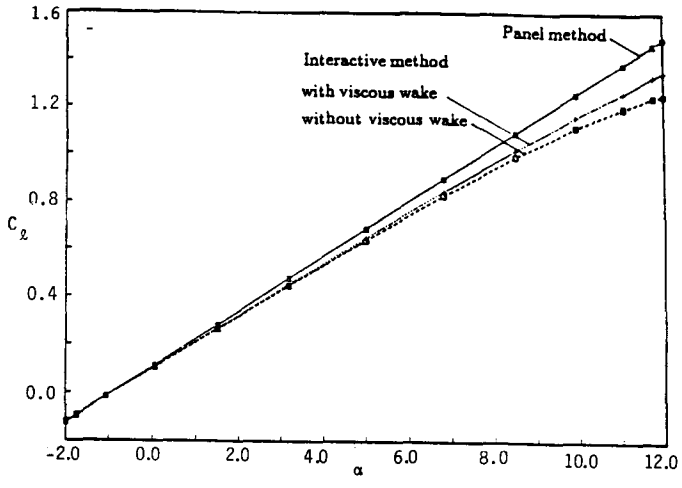

(a)

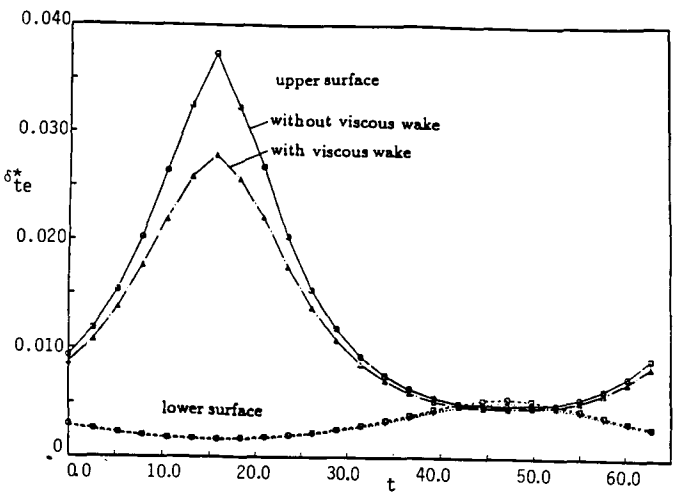

(b)

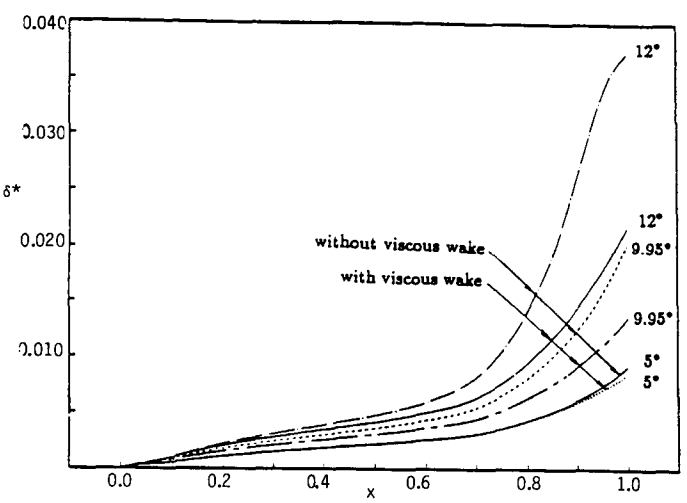

(c)

Fig. 3. The effect of viscous wake on (a) lift-coefficient and (b) displacement-thickness distribution at trailing edge and (c) displacement-thickness distribution on the upper surface. $\alpha(t) = 5° + 7° \sin(\omega t)$, $k = 1 \times 10^{-5}$, $R_c = 2 \times 10^6$.

3.1 Results for Steady Flows

Steady-flow calculations including the wake effect were performed for a Sikorsky SSC-A09 airfoil at a chord Reynolds number of 2×10^6 with transition fixed on the upper and lower surfaces at locations two stations behind the stagnation point. These results have been described before by Cebeci and Jang (1990) and therefore only a few additional comparisons with the measurements of Lorber and Carta (1988) are presented here.

Pressure-coefficient distributions on the airfoil surface are displayed in Figs. 4a to 4d. At low angles

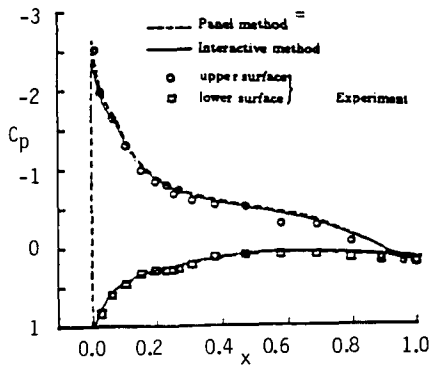

(a)

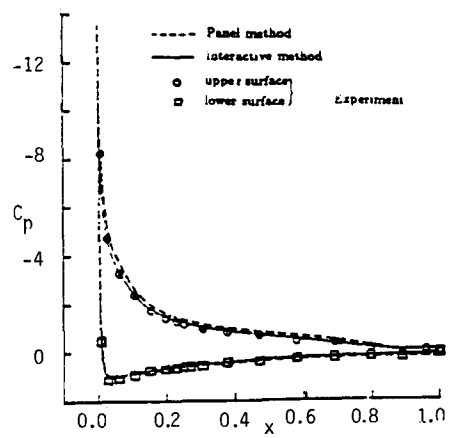

(b)

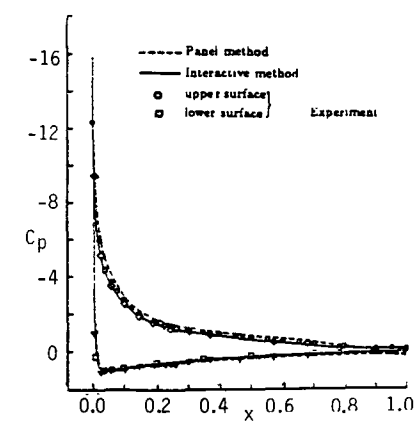

(c)

Fig. 4. Pressure-coefficient distributions at α = (a) 6°, (b) 13°, (c) 14°, (d) 15°. - Steady, $R_c = 2 \times 10^6$.

Downloaded From: https://proceedings.asmedigitalcollection.asme.org on 01/24/2019 Terms of Use: http://www.asme.org/about-asme/terms-of-use

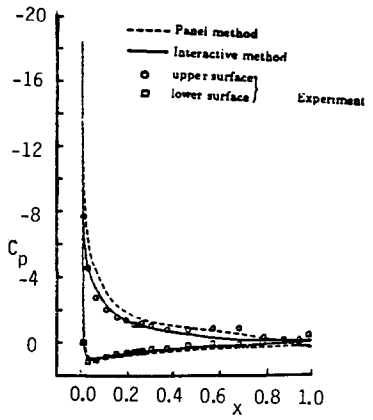

(d)

Fig. 4. Continued.

of attack, the boundary-layer effects are negligible and the results of both the panel and interactive methods agree with experiment. When the angles of attack are higher than 13 degrees, the boundary-layer effects become more important, and Figs. 4c to 4d show that the interactive solutions agree with experimental data better than those of inviscid-flow equations.

3.2 Results for Unsteady Flows

The accuracy of an interactive method for simulating the unsteady flow depends on several factors which include the inviscid-flow method, the modification of the inviscid-flow method to accept viscous effects, the boundary-layer scheme as well as the numerical scheme used to solve the equations, and the coupling procedure between the inviscid- and viscous-flow calculations. The results in the previous subsection described for steady flows show that these factors are properly represented in the steady-flow calculations so that the steady-flow model can now be used as a base for extension to unsteady-flow calculations.

The overall features of a subsonic flow over an airfoil executing an unsteady motion are primarily characterized by the extent of flow reversal (or separation). For testing the performance of our method, calculations are performed in the order of increasing levels of flow complexity, starting first with flows without and then with reversal and in subsection 3.3 are followed by flows with substantial regions of flow separation.

Flows Without Reversal Region. We again consider the same Sikorsky airfoil in which the change in angle of attack takes place according to

$$\alpha(t) = 5° + 5° \sin\omega t$$

at three reduced frequencies, $k = 1 \times 10^{-4}$, 0.1 and 0.5 for a chord Reynolds number of 2×10^6. The interactive flow calculations are performed with the unsteady panel method and the inverse boundary-layer method described in Section 2.0.

The results with the interactive method shown in Fig. 5 were first obtained with the inverse boundary-layer calculations performed for steady flow calculations. Even though at each time the inviscid flow was calculated with the unsteady panel method, the viscous effects were calculated with the boundary-layer equations in which the time-dependent terms, $\partial u/\partial t$ and $\partial u_e/\partial t$ were neglected. This quasi-steady model is valid when

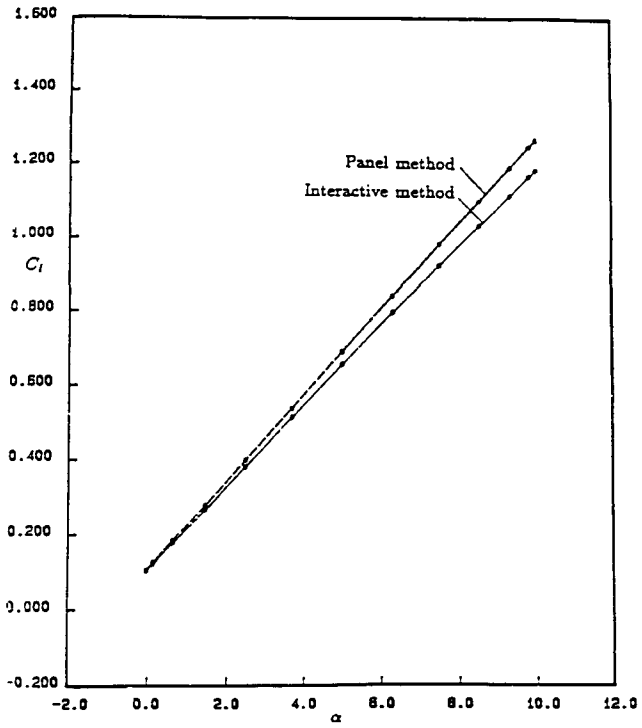

(a)

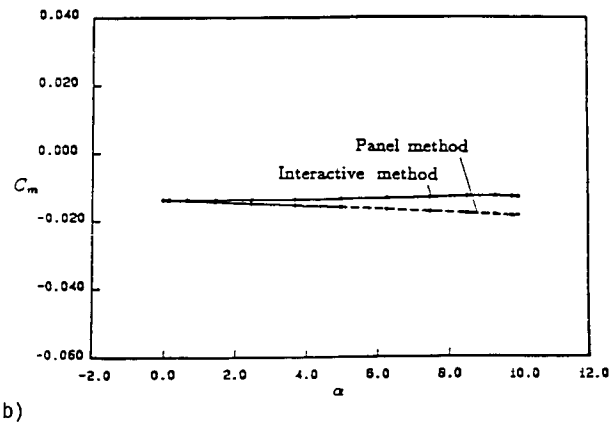

(b)

Fig. 5. Variations of (a) lift and (b) pitching moment coefficients with angle of attack for the SSC-A09 airfoil. $\alpha(t) = 5° + 5° \sin(\omega t)$, $k = 10^{-4}$.

$$\frac{\partial u}{\partial t} \text{ and } \frac{\partial u_e}{\partial t} \ll u_e \frac{\partial u_e}{\partial x}$$

Repeating the calculations in which the viscous effects are computed with the unsteady boundary-layer equations and comparing the results with those obtained with the quasi-steady model showed that (Fig. 5) the solutions of both interactive methods were identical.

Figures 6 and 7 show the lift and pitching moment coefficient curves for the other two frequencies, all computed with viscous effects obtained from the solutions of the unsteady boundary-layer equations. We can see from the results that the hysteresis effects increase with the increase of the reduced frequency. Since the boundary-layer calculation started from steady state and suddenly joined the inviscid flow

Downloaded From: https://proceedings.asmedigitalcollection.asme.org on 01/24/2019 Terms of Use: http://www.asme.org/about-asme/terms-of-use

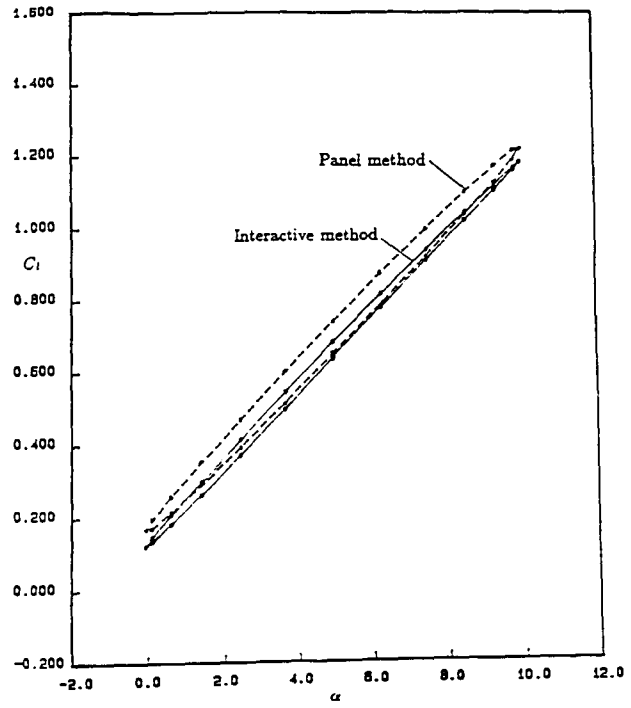

(a)

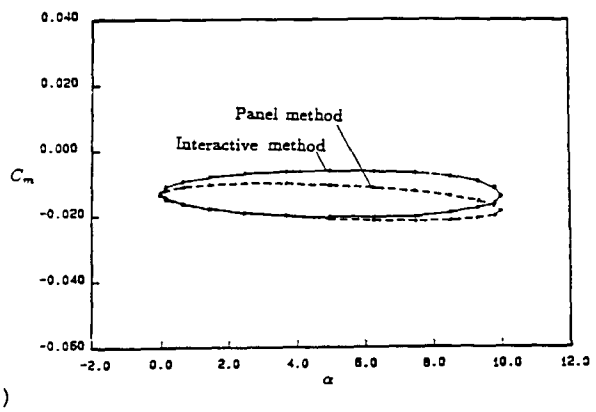

(b)

Fig. 6. Variations of (a) lift and (c) pitching moment coefficients of the SSC-A09 airfoil with angle of attack. $\alpha(t) = 5° + 5° \sin(\omega t)$, $k = 0.1$.

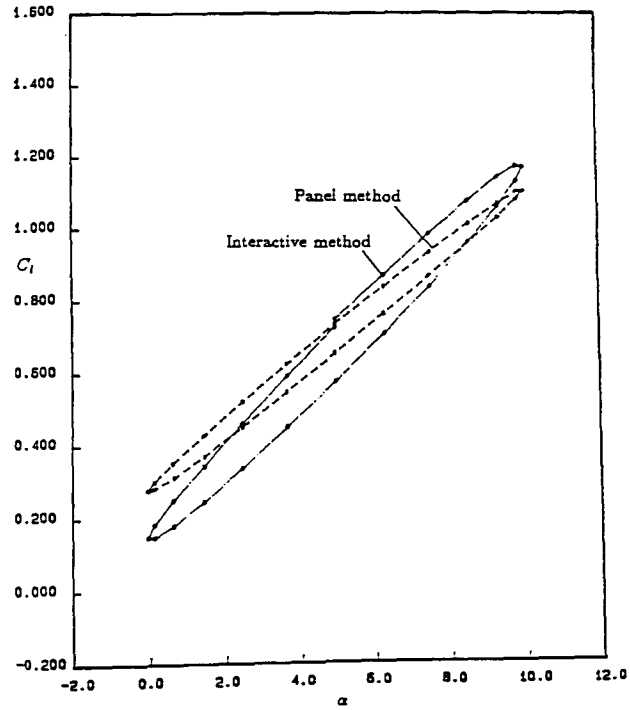

(a)

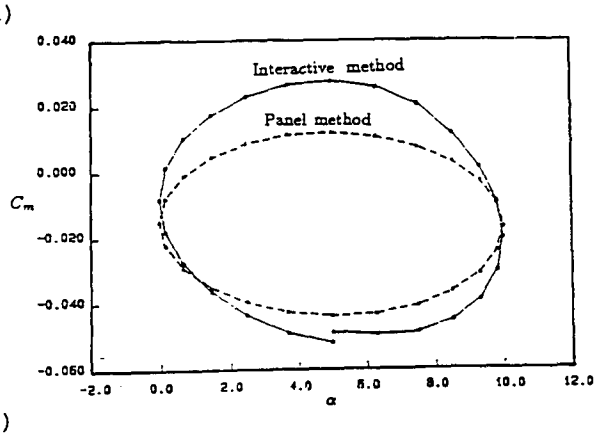

(b)

Fig. 7. Variations of (a) lift and (b) pitching moment coefficients of the SSC-A09 airfoil with angle of attack. - Unsteady, $\alpha(t) = 5° + 5° \sin(\omega t)$, $k = 0.5$.

calculation, the viscous-inviscid results showed a little discontinuity at the beginning and the end of the cycle. One very interesting aspect of the lift coefficient curve is that at $k = 0.1$ the lift coefficient of the upward stroke is lower than that of the downward stroke, but it is just opposite at $k = 0.5$. This phenomenon can be explained by comparing the pressure coefficient distributions in the upward and downward strokes at a certain angle of attack ($\alpha = 7.5°$ purely inviscid flow, for example), as shown in Fig. 8 for different frequencies. At $k = 10^{-4}$, no hysteresis effects appear and the pressure-coefficient distributions of upward and downward strokes are identical to the steady one. Increasing k to 0.1, the hysteresis effects appear mainly on the fore part of the airfoil. The pressure peak at $\alpha = 7.5° \uparrow$ is lower than the corresponding steady one, whereas that at $\alpha = 7.5° \downarrow$ is higher, so that the lift coefficient in the downward stroke is higher than that in the upward stroke. Increasing k generates more unsteady motion of the airfoil aft (since it is farther from the pivot point) so that the effects on the pressure distribution there are more enhanced, as shown in Fig. 8c, for $k = 0.5$. From the pressure distribution, we can see that in the downward stroke the negative contribution to the lift coefficient in the aft part cannot be balanced by the positive contribution from the fore part so that the C_ℓ in the downward stroke is lower.

When an airfoil performs an unsteady motion, there is energy transfer between the airfoil and its surrounding fluid, and this energy transfer is indicated by the pitching moment. The pitching moment at $k = 0.1$ within one cycle of motion is shown in Fig. 6b. The negative pitch moment in the upward stroke indicates that the airfoil motion is against the aerodynamic moment induced by the surrounding fluid, whereas in the

Downloaded From: https://proceedings.asmedigitalcollection.asme.org on 01/24/2019 Terms of Use: http://www.asme.org/about-asme/terms-of-use

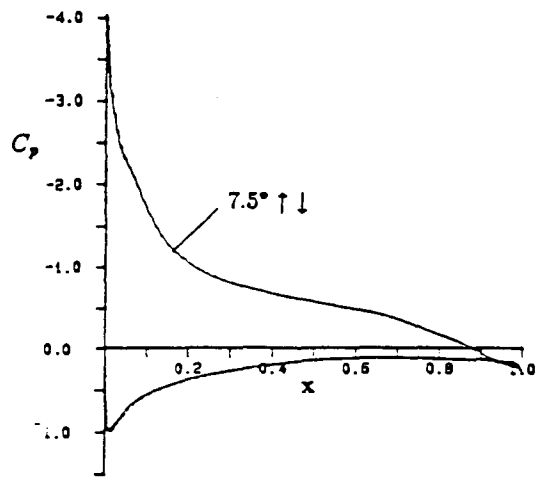

(a)

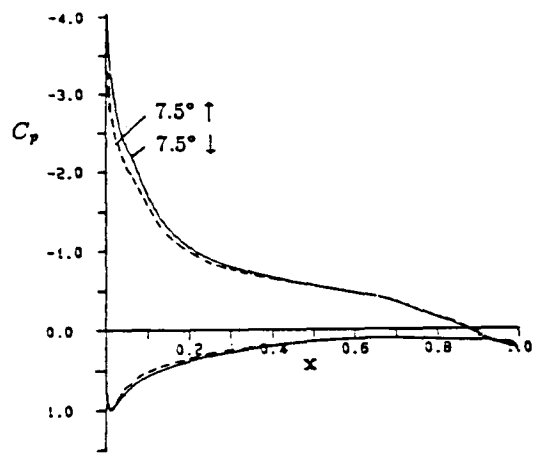

(b)

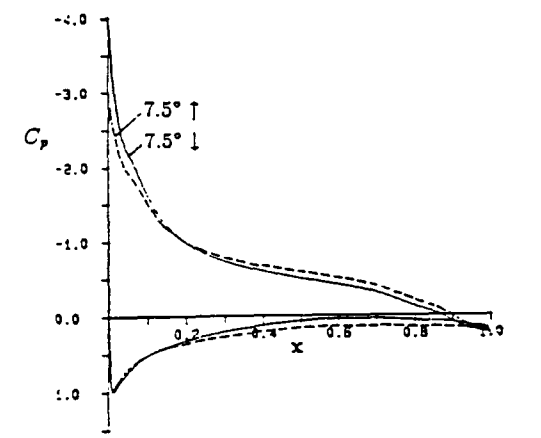

(c)

Fig. 8. The inviscid-flow pressure-coefficient distributions for the SSC-A09 airfoil at α = 7.5° of the harmonic oscillation, $\alpha(t)$ = 5° + 5° sin(ωt), with k = (a) 10^{-4}, (b) 0.1, and (c) 0.5.

downward stroke the aerodynamic moment is favorable to the airfoil motion. Therefore, the energy is transferred to and absorbed from the fluid in the upward and the downward strokes, respectively. The area enclosed by the pitch-moment curve indicates the net energy transferred to the fluid in each cycle of harmonic oscillation. The viscosity enhances the hysteresis effects, Fig. 6b, so that more energy is required to execute a cycle of motion. In the very slow pitching case, k = 10^{-4}, both the inviscid and the viscous-inviscid interactive curves show almost no hysteresis effects, Fig. 5b, so that the energy transferred to the fluid in one cycle is negligible. At k = 0.5, the pitch moment in most of the downward stroke becomes positive, which indicates that the airfoil motion is against the aerodynamic moment not only in the upward stroke but also in most of the downward stroke. In this case, the viscosity also increases the hysteresis effects and the energy transferred to the surrounding fluid in one cycle of motion.

The boundary-layer development can be represented by the displacement thickness distributions; some features of them are displayed in Figs. 9 and 10. The displacement thickness distributions on the upper and lower sides of the airfoil and wake at angles of attack α = 5°, 7.5° and 10° in the upward and downward strokes are shown in Fig. 9 for k = 0.5. At a certain angle of attack, the upper-side displacement thickness in the downward stroke is higher than that in the upward stroke. The influence of the reduced frequency on the displacement-thickness distribution can be clearly represented by the trailing-edge value, as shown in Fig. 10. The maximum displacement thickness shifts to the downward stroke as the reduced frequency increases, as in steady flows discussed in the previous section.

Flows with Reversal Region. In the upward stroke of the harmonic oscillation, the pitch rate decreases when the airfoil approaches the maximum angle. At high angles of attack, decreasing the pitch rate speeds up

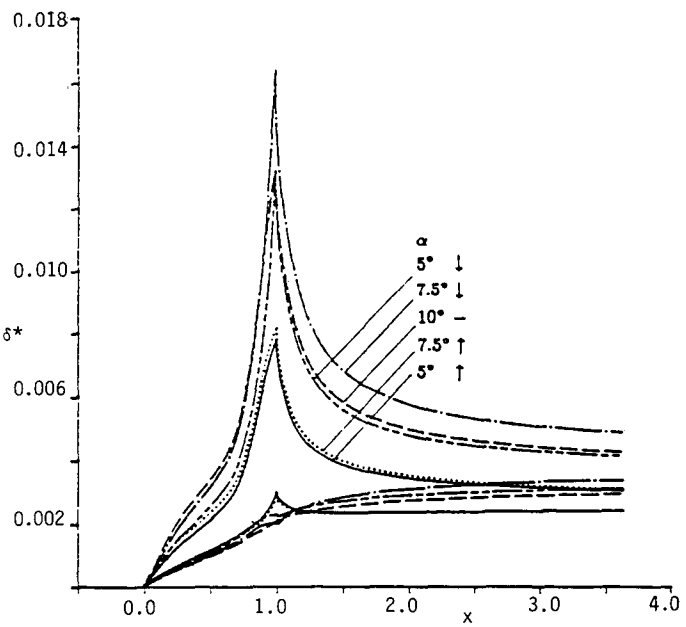

Fig. 9. Comparison of the displacement-thickness distributions of the SSC-A09 airfoil in the upward and downward strokes.

Downloaded From: https://proceedings.asmedigitalcollection.asme.org on 01/24/2019 Terms of Use: http://www.asme.org/about-asme/terms-of-use

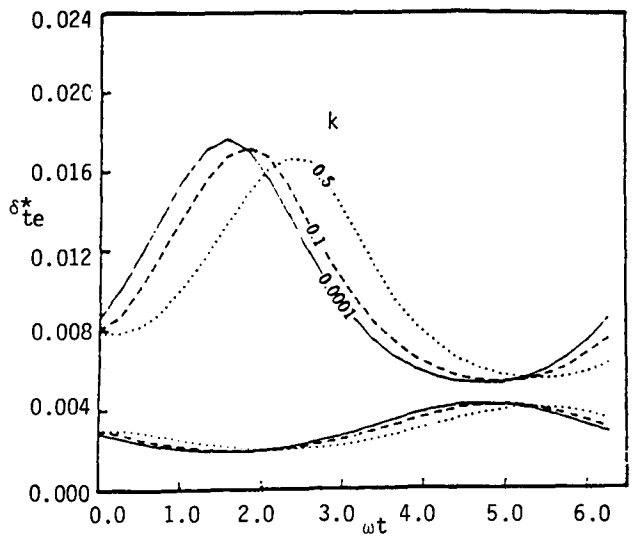

Fig. 10. The effect of reduced frequency on the trailing-edge displacement thicknesses of the SSC-A09 airfoil.

the rate of expansion of the trailing-edge reversal or separation region. To suppress this region and delay the occurrence of stall, a high pitch rate must be maintained at high angles of attack. To study the behavior of an airfoil under these conditions we consider the same airfoil executing a ramp-type motion from 5° to 16° with a constant pitch rate of A ($\dot{\alpha}$ c/ u_∞) = 0.02.

In Fig. 11, the lift-coefficient curves computed by using the unsteady and quasi-steady approaches for A = 0.02 are compared with the solution computed by the quasi-steady approach for A = 10^{-5}. The quasi-steady solution at A = 0.02 has a higher maximum lift at higher angle of attack than that at A = 10^{-5}. Due to the retarding effects from the lower angle of attack and smaller streamwise pressure gradient, the unsteady-flow solution shows no stall within the angles of attack computed. Figures 11b and 11c display the displacement-thickness distributions for two angles of attack. At an angle of attack before static stall, α = 13°, the differences between the three distributions in Fig. 11b are much less than those shown in Fig. 11c for the solutions after static stall at α = 15°. The variation of displacement thickness with the reduced frequency can be represented by the trailing edge values, Fig. 12. From Figs. 11b, 11c and 12, we can conclude that increasing the pitch rate reduces the displacement thickness on the upper side of the flow-field and hence the boundary-layer effects on the outer inviscid flow.

The local skin-friction coefficient distributions on the upper and lower surfaces of the airfoil computed with the quasi-steady approach at α = 13° are shown in Fig. 13. The C_f distribution on the lower surface are influenced very little with pitch rate, but those on the upper surface are influenced with the reversal region suppressed by the increasing pitch rate. Figure 15 shows the results in which the boundary-layer calculations are performed with unsteady mode for A = 0.02. With increase in angle of attack, the friction coefficient on the upper surface decreases, whereas on the lower surface it increases, and a reversal flow region starts growing from the

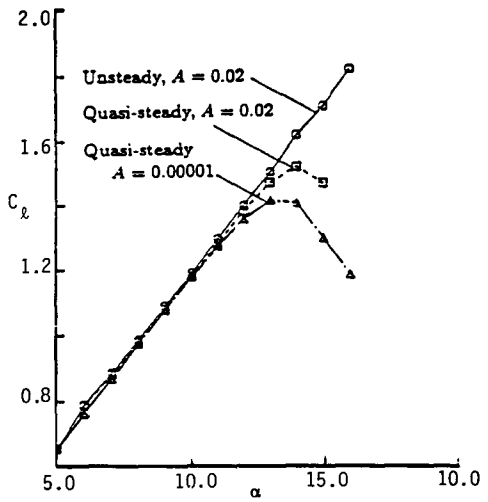

(a)

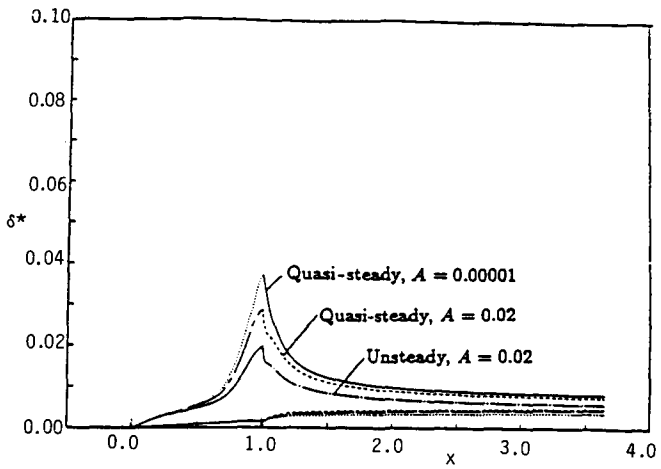

(b)

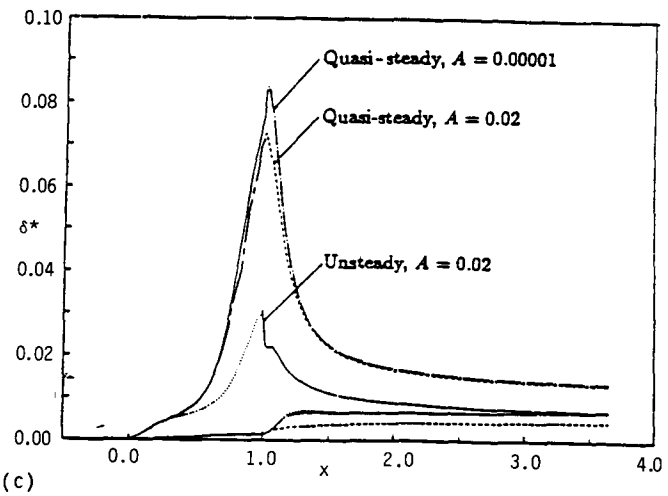

(c)

Fig. 11. The effects of pitch rate and the boundary-layer approach on the (a) lift-coefficient and (b) α = 13°, (c) α = 15° distributions of the SSC-A09 airfoil subject to ramp-type motion with constant pitch rate.

Downloaded From: https://proceedings.asmedigitalcollection.asme.org on 01/24/2019 Terms of Use: http://www.asme.org/about-asme/terms-of-use

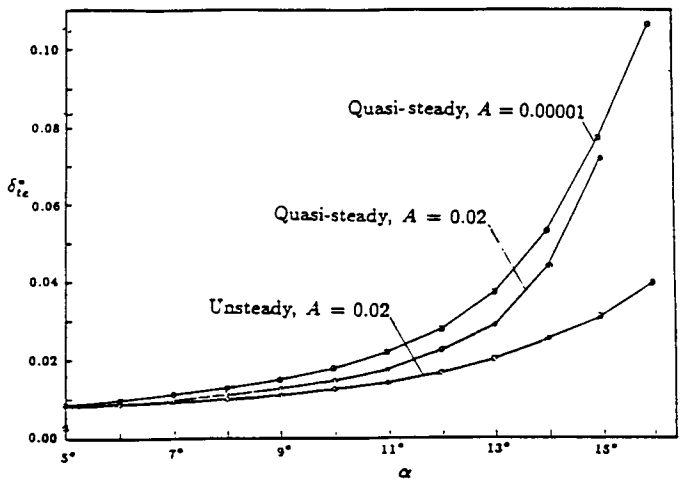

Fig. 12. The effects of pitch rate and the boundary-layer approach on the trailing-edge displacement-thickness distribution of he SSC-A09 airfoil subject to a ramp-type motion with constant pitch rate.

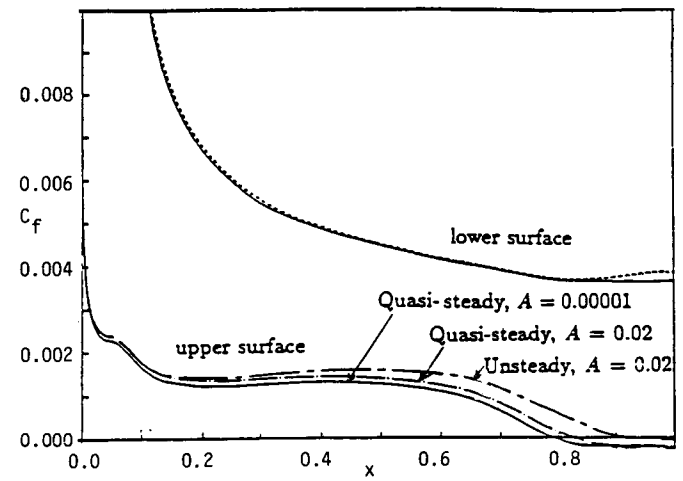

Fig. 13. The effects of pitch rate and the boundary-layer approach on the local skin-friction coefficient distribution of the SSC-A09 airfoil subject to a ramp-type motion with constant pitch rate.

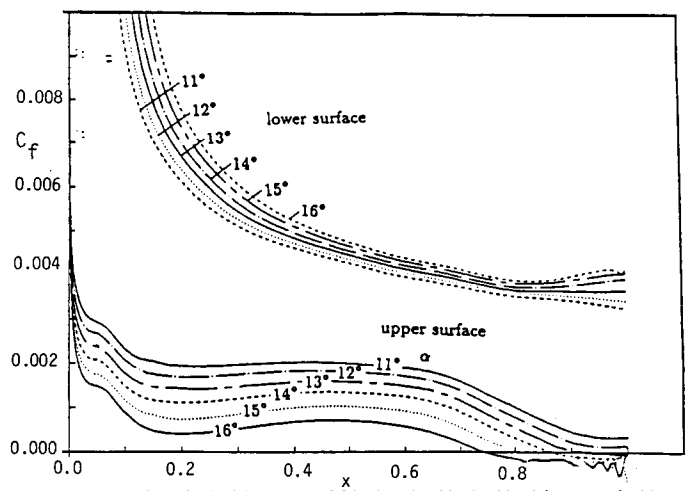

Fig. 14. The friction-coefficient distributions of the SSC-A09 airfoil subject to a ramp-type motion with constant pitch rate, A = 0.02.

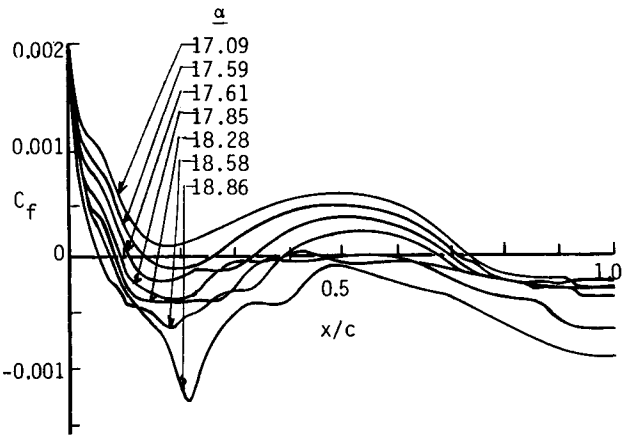

Fig. 15. Initiation of leading-edge vortex with trailing-edge separation on the Sikorsky airfoil subject to ramp-type motion with a pitch rate of 0.02, $R_c = 2 \times 10^6$, α varies from 0° to 30°.

trailing edge at the angle of attack of 12.7°. The wiggle on the C_f distribution near the trailing edge is enhanced as the reversal region increases. The extension of the calculation method requires a procedure which is able to avoid the wiggles in the solutions. This will be discussed in the next subsection.

3.3 Initiation of Dynamic Stall on a Pitching Airfoil

The numerical solution of the unsteady boundary-layer equations for two-dimensional flows is a relatively easy task provided there are not flow reversals in the streamwise velocity component u. Keller's box scheme used in this paper, or any other finite-difference method such as the Crank-Nicolson scheme, can be used to solve the equations for a prescribed pressure distribution. This is not the case, however, when the streamwise velocity component contains negative velocities. While there are some remedies to circumvent the difficulties in the solution procedure caused by flow reversals in u, they are not satisfactory when there are substantial regions of flow reversals. As discussed by Cebeci (1986), their calculation requires a numerical method which follows the physics of the flow and proper choice of step sizes in time and x-directions. An appropriate scheme that can be used to satisfy these requirements is the characteristic box scheme developed by Cebeci and Stewartson, described by Bradshaw et al. (1981), and used here to extend the unsteady flow calculations of the previous subsection to higher angles of attack.

The results using this scheme with special attention to the choice of step lengths are presented for the Sikorsky airfoil subject to the ramp-type of motion with a pitch rate of 0.02. The experimental data, which is due to Lorber and Carta (1988), indicates that the vortex initiates around 18 to 19 degrees of angle of attack. The calculations confirm this and indicate how the trailing-edge separation causes the initiation of the vortex. To elaborate further on this point, let us consider the distribution of the local skin-friction values on the upper surface of this airfoil at several angles of attack, Fig. 15. It is clear from Fig. 14 that for $\alpha < 12°$, there is no flow separation on the airfoil which has a steady stall angle of around 14°. The unsteadiness causes the stall angle to increase to around 30°, according to experiments. The flow behavior on the airfoil begins to change quickly, however, once the trailing-edge separation takes place for

Downloaded From: https://proceedings.asmedigitalcollection.asme.org on 01/24/2019 Terms of Use: http://www.asme.org/about-asme/terms-of-use

$\alpha > 12°$, see Fig. 14. At $\alpha = 17.09$, there is no leading-edge flow separation but only a trailing-edge separation which occurs around 72%. At the next angle of attack, $\alpha = 17.69$, leading-edge separation takes place close to 12% chord with a bubble reattaching around 33% and is followed by a trailing-edge separation at 70%. The explosive nature of the leading-edge separation bubble, which is all turbulent, becomes more obvious at the next $\alpha = 17.88$, where leading-edge separation takes place around 10% but the reattachment of the bubble moves to 50% chord, a bubble of 40% in extent, followed by trailing-edge separation moving to 60% chord. Very shortly thereafter, less than one degree increase in angle of attack, the leading-edge separation bubble disappears with complete flow separation taking place at around 5% chord.

4.0 CONCLUDING REMARKS

An interactive boundary-layer method for computing unsteady incompressible flows over airfoils, including the initiation of dynamic stall, is described. The inviscid unsteady panel method, developed by Platzer and Teng, is further extended to include viscous effects. The boundary-layer method uses an inverse finite-difference technique based on Keller's box schemes and the algebraic turbulence model of Cebeci and Smith. Following the description of the method, it has been applied to unsteady flows in order to investigate the abilities of the method and compare the calculations with available experimental data. The study shows that: (a) In the harmonic oscillation cases, hysteresis effects are evident as the reduced frequency increases. The hysteresis phenomena appear in the solutions of both viscous and inviscid flows and are qualitatively represented by the present method. (b) In the case of ramp-type motion with a high constant pitch rate, the solutions correctly show that the thick trailing-edge separation region in steady flow is suppressed to a thin reversal region and, at the same time, stall is delayed. (c) Due to the neglect of unsteady terms, $\partial u/\partial t$ and $\partial u_e/\partial t$, the quasi-steady approach does not properly simulate unsteady flows at high pitch rates. (d) The prediction of the onset of dynamic stall with the present method agrees with the data of Lorber and Carta for the Sikorsky airfoil and shows that for this airfoil, the initiation of dynamic stall is caused by the trailing-edge separation.

Ackowledgement: This work was performed under Grant AFOSR-900262.

5.0 REFERENCES

Basu, B.C. and Hancock, G.J., 1987, "The Unsteady Motion of a Two-Dimensional Airfoil in Incompressible Inviscid Flow," Journal of Fluid Mechanics, Vol. 87, p. 157-168.

Bradshaw, P., Cebeci, T. and Whitelaw, J.H., 1981, Engineering Calculation Methods for Turbulent Flows, Academic Press, NY.

Carr, L.W., 1988, "Progress in Analysis and Prediction of Dynamic Stall," Journal of Aircraft, Vol. 25, No. 1, pp. 6-17.

Cebeci, T., 1986, "Unsteady Boundary Layers with an Intelligent Numerical Scheme," Journal of Fluid Mechanics, Vol. 163, pp. 129-140.

Cebeci, T. and Carr, L.W., 1983, "Calculation of Boundary Layer Near the Stagnation Point of an Oscillating Airfoil," NASA TM 84350.

Cebeci, T. and Khattab, A.A., 1992, "Numerical Solution of the Unsteady Boundary-Layer Eqautions with Extensive Regions of Flow Separation," paper in preparation.

Cebeci, T. and Jang, H.M., 1990, "Interactive Boundary-Layer Method for Unsteady Airfoil Flows: Quasi-Steady Model," Journal of Aircraft, pp. 673-678.

Cebeci, T. and Smith, A.M.O., 1974, Analysis of Turbulent Boundary Layers, Academic Press, NY.

Cebeci, T., Jau, J., Vitiello, D. and Chang, K.C., 1990, "Prediction of Post-Stall Flows on Airfoils," in Numerical and Physical Aspects of Aerodynamic Flows IV (ed. T. Cebeci), Springer-Verlag, Heidelberg, p. 93.

Cebeci, T., McIlvaine, M., Chen, H.H. and Liebeck, R.H., 1991, "Calculation of Low Reynolds Number Flows at High Angles of Attack," Journal of Aircraft, Vo. 28, No. 4, pp. 246-252.

Cebeci, T., Clark, R.W., Chang, K.C., Halsey, N.D., and Lee, K., 1986, "Airfoils with Separation and the Resulting Wakes," Journal of Fluid Mechanics, No. 163, pp. 323-347.

Chang, K.C., Alemdaroglu, N., Mehta, U. and Cebeci, T., 1988, "Further Comparisons of Interactive Boundary-Layer and Thin-Layer Navier-Stokes Procedures," Journal of Aircraft, Vol. 25, pp. 897-903.

Hess, J.L. and Smith, A.M.O., 1966, "Calculation of Potential Flow about Arbitrary Bodies," in Progress in Aeronautical Sciences, Pergamon Press, Oxford, Vol. 8, pp. 1-138.

Jang, H.M., Ekaterinaris, J.A., Platzer, M.F., Cebeci, T., 1991, "Essential Ingredients for the Computation of Steady and Unsteady Blade Boundary layers," ASME Journal of Turbomachinery, Vol. 13, pp. 608-616.

Lorber, P.F. and Carta, F.O., 1988, "Airfoil Dynamic Stall at Constant Pitch Rate and High Reynolds Number," Journal of Aircraft, pp. 548-556.

Mehta, U., Chang, K.C. and Cebeci, T., 1986, "Relative Advantages of Interactive and Thin Navier-Stokes Procedures," in Numerical and Physical Aspects of Aerodynamic Flows III (ed. T. Cebeci), Springer-Verlag, New York.

Teng, N.H., 1987, "The Development of a Computer Code (U2DIIF) for the Numerical Solution of Unsteady, Inviscid and Incompressible Flow Over an Airfoil," M.S. Thesis, Naval Postgraduate School, Monterey, CA.

Veldman, A.E.P., 1981, "New, Quasi-Simultaneous Method to Calculate Interacting Boundary Layers," AIAA Journal, Vol. 154, pp. 79-85.

Downloaded From: https://proceedings.asmedigitalcollection.asme.org on 01/24/2019 Terms of Use: http://www.asme.org/about-asme/terms-of-use